AAS 19-471

IMPACT OF INTERNAL HEATING ON SPACECRAFT THERMAL SIGNATURE

Scott Carnahan,* Hanspeter Schaub,† Benjamin Lane ‡

Vision-based relative navigation of spacecraft in the thermal infrared is a burgeoning area of research. The asymmetry of spacecraft thermal systems could be used to identify the attitude of a symmetric object using the infrared spectrum that would be challenging in the visible spectrum. Spacecraft internal thermal signatures have not been focused on in thermal relative navigation research. In order to investigate this, two simulation tools are built for the Basilisk astrodynamics framework developed by the Autonomous Vehicle System lab at CU Boulder. The first is a thermal modeling package. The second is a thermal camera module which allows for closed-loop image generation of spacecraft with thermal system models. The closed-loop capability of the camera is unique among spacecraft thermal image simulation tools. The camera and thermal package are demonstrated together in a closed-loop two-spacecraft dynamics scenario.

INTRODUCTION

Vision-based relative navigation is an active area of research for non-cooperative rendezvous and active debris removal. Infrared vision based navigation has gained more interest in the past few years due to the potential of clear imaging regardless of external illumination of the target.[1] Various tools exist to model spacecraft thermal signatures. The Spacecraft Imaging Simulation Environment (SISE), based on an earlier visible-spectrum spacecraft image simulator, produces thermal spacecraft images by post-processing multi-spacecraft dynamics simulations.[2,3] The Spacecraft Controls Toolbox (SCT) by Princeton Satellite systems offers a thermal toolbox that includes thermal image generation. SCT is intended for first order analysis and is a commercial software. The Adaptive Thermal Modeling Application for Small Satellites (ATMA) provides thermal modeling capability but not thermal image generation.[4] Garnier et al provide an infrared sensor model which is aimed at realistically modeling the physics of sensor, rather than dynamics and navigation integration.[5] Common spacecraft thermal analysis tools like Thermal Desktop and MATLAB Simulink provide general tools for thermal analysis, but none have tools aimed at providing thermal images for use by navigation systems.

In both infrared and visible spectra, a plethora of model and image matching algorithms are feasible for spacecraft recognition.[2,6,7] Detailed infrared imaging of spacecraft in all lighting conditions

*Draper Graduate Fellow, Department of Aerospace Engineering Sciences, University of Colorado, 431 UCB, Colorado Center for Astrodynamics Research, Boulder, CO 80309-0431

†Professor and Glenn L. Murphy Endowed Chair of Engineering, Department of Aerospace Engineering Sciences, University of Colorado, 431 UCB, Colorado Center for Astrodynamics Research, Boulder, CO 80309-0431. AAS Fellow

‡Group Leader, Advanced Position, Navigation & Timing Instrumentation, 555 Technology Square, Cambridge, MA 02139

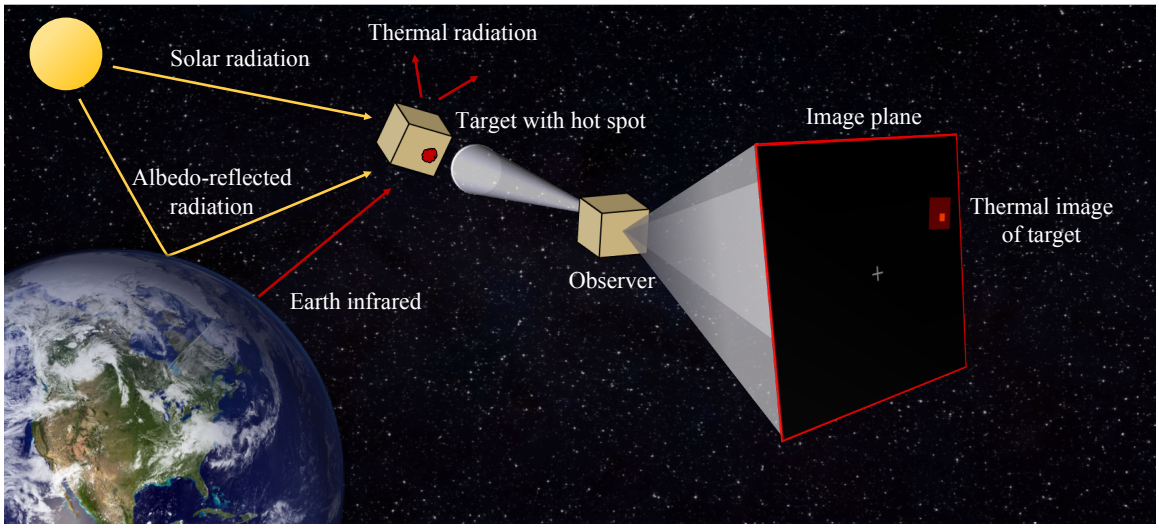

Figure 1. A thermal imaging scenario. The target experiences external thermal influences and has internal thermal asymmetry. The observer has a thermal camera to image the target.

is possible on active space missions.[8] One challenge remaining in infrared-based attitude determination of non-cooperative spacecraft is resolving ambiguities due to spacecraft symmetry. Previous work gets around this problem by assuming a "close enough" initial guess for target attitude to avoid incorrect local minima in the matching algorithms.[6,7] This is not likely possible for tumbling spacecraft, debris, or spacecraft about which very little is known. This work aims to address the issue of attitude ambiguity by enabling the incorporation of additional infrared-visual information due to internal thermal systems.

For vision-based relative navigation in the infrared, external asymmetries of the target such as antennae or booms could be used to resolve attitude ambiguities if high resolution imaging and modeling is available. However, even resolution as high as demonstrated by Shi may not capture fine details that are necessary.[9] Furthermore, on-board model-matching algorithms are likely to use low-fidelity models which remove asymmetric details.[6] Either or both of these limitations exacerbate the attitude ambiguity due to spacecraft symmetry. One solution is to use spacecraft thermal system asymmetry to resolve attitude ambiguities. If target thermal design includes heat dumping to the spacecraft body, a hot-spot could be visible in the thermal infrared which would accurately identify the spacecraft attitude as seen by infrared cameras. Alternatively, for tumbling and inactive spacecraft heated by the sun, internal structural asymmetry could provide the signature needed. Additionally, in dynamic illumination conditions, thermal inertia will have a sizable effect on the time-varying infrared signature of a spacecraft. This necessitates dynamic thermal testing.

Testing the idea of using internal thermal asymmetry for attitude determination requires either in-space, laboratory, or simulated experiments. Laboratory and in-space experiments provide strong validation and data for the test cases investigated. Simulation allows closed-loop testing of navigation and control based on generated thermal images in many different environments with multiple navigation algorithms, but simulation must be thoroughly validated. To this end, a thermal camera

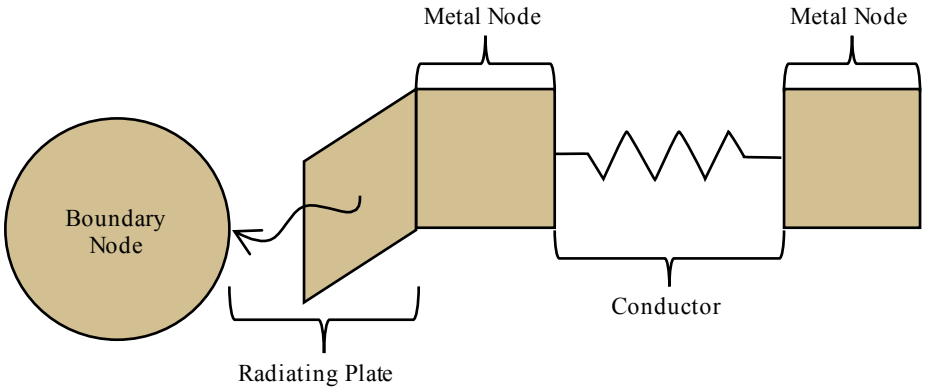

Figure 2. An example thermal network. Each of the elements mentioned in the figure can be modeled as an instance of the modules described below.

module is developed in the Basilisk astrodynamics framework* developed by the Autonomous Vehicle Systems (AVS) lab at CU Boulder. Other work in the AVS lab uses vision-based navigation (in the visible spectrum) in Basilisk, so some synergy is expected.[10] In order to generate accurate thermal images, a lumped parameter thermal network solver is created. The lumped parameter system provides the modularity to model any system desired in a timely manner. Other methods may provide higher fidelity (finite-element thermal modeling) results but at the cost of modularity and computation speed. The package as designed can handle arbitrarily complex thermal systems with internal, external, and environmental thermal effects. The camera is developed to use the thermal system outputs and a common plotting library to generate thermal images. This camera module projects polygon vertices into the image plane rather than a collection of surface points as in SISE.[3] The advantage of using Basilisk is that a formation of 6-DOF spacecraft can be simulated with standard Basilisk modules that are already validated, which reduces the validation cost for the thermal modules. With the additions in this work, a thermal system can be modeled on a target spacecraft while a camera is modeled on a separate observer spacecraft. Thermodynamic properties and images can be updated closed-loop and combined with navigation and control algorithms.

The following sections discuss the basic thermal network implementation along with some utilities to mesh a spacecraft surface. This is followed by the infrared camera implementation. Then, a scenario is demonstrated in which a target spacecraft (with a thermal system) and an observer spacecraft (with a thermal camera) fly past each other as seen in Figure 1.

THERMAL NETWORK MODULES

The thermal network consists of conductor, metal node, and radiating plate modules. The simulation allows for external thermal inputs like solar, reflected sunlight due to albedo, and planetary infrared radiation as well as internal thermal inputs like battery waste heat, resistive heaters, and computer waste heat. The radiating plates output heat which completes the system energy balance. Thus, a faceted spacecraft model can be made to represent external geometry which is connected to internal thermal dynamics by building a network of conductors, metal nodes, and radiating plates.

The thermal modules are generally separable into three categories: spacecraft internal, spacecraft

*`http://hanspeterschaub.info/bskMain.html`

external, and environment. A thermal system module handles interactions between other modules in the network. The method used to solve transient thermal networks is sometimes called a lumped capacitance model in analogy to electrical resistance network modeling. The method is laid out in detail in the NASA Thermal Network Modeling Handbook, which has since been reformatted by K&K Associates.[11,12] Other sources are also available. The thermodynamic formulation of modules (like conductors) varies by implementation and source. Spacecraft internal, spacecraft external, and environmental thermal models are described in the next three sections.

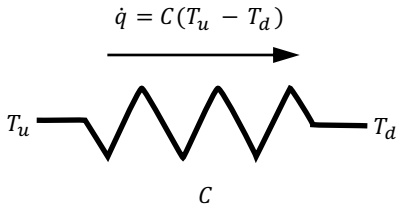

Figure 3. All thermal paths, including the conductor, are connected to an upstream and downstream temperature source. Heat flows from up to down.

Spacecraft Internal

Conductor The thermal conductor, illustrated in Figure 3, calculates the heat flow rate between two thermal nodes via the equation:

$$\dot{q} = C(T_u - T_d) \tag{1}$$

where T_u is the upstream node temperature in Kelvin, T_d is the downstream node temperature in Kelvin, C is the conductance (inverse resistance) in Joules per Kelvin per second, and $\dot{q}$ is the heat flow rate in Joules per second. Temperatures are provided to the conductor by the thermal system. A conductance factor, C, is different from and a function of conductivity. Heat rate is considered positive from up to down. Node net heat rates are considered positive into the node. Therefore, conductor heat flow (magnitude) is subtracted from upstream nodes and added to downstream nodes when node net heat rates are summed.

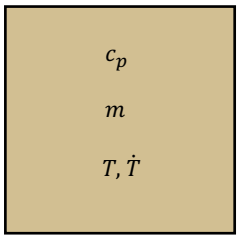

Figure 4. Thermal nodes, including the metal node, can be attached to an arbitrary number of thermal paths. Nodes have thermal properties and integrate temperature.

Metal Node The metal node module is responsible for calculating the temperature rate of a node given the heat rate through surrounding thermal paths. It has a mass, m, and specific heat, c_p, which are taken as constants. The temperature rate, $\dot{T}$, in a node is proportional to the total heat rate into the node

$$\dot{T} = \frac{\sum_i^n \dot{q}_i}{mc_p} \tag{2}$$

where n is the number of of thermal paths attached to the node. Temperature is integrated with an Euler method

$$T_k = T_{k-1} + \dot{T}_{k-1}\Delta \mathrm{t} \tag{3}$$

where k is the current simulation step and Δt is the time step in seconds. Finally, energy, Q, is integrated in all nodes so that system energy can be tracked for conservation. This tracks the net energy into the system over time rather than an absolute measure of energy in the system.

$$Q_k = Q_{k-1} + \dot{q}_{k-1}\Delta \mathrm{t} \tag{4}$$

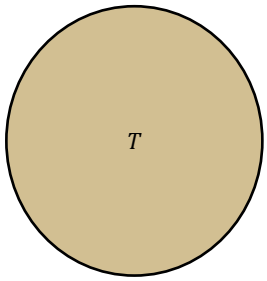

Figure 5. Boundary nodes are outside of the system and have constant temperature. Energy can be exchanged with the system via any thermal path.

Boundary Nodes The temperature state for any node can be turned off. This renders it external to the system. In this case it is a boundary node. Energy in and out of the boundary node is considered as crossing the system boundary. Unless they are manually altered throughout the simulated, boundary node temperatures remain constant.

Spacecraft External

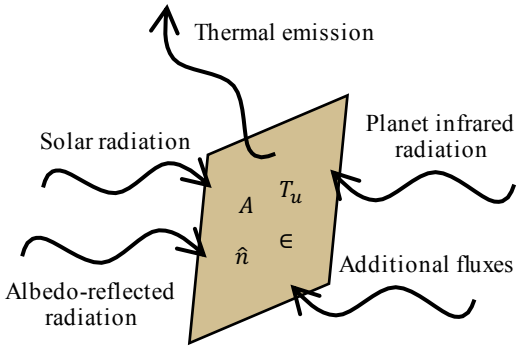

Figure 6. Radiating plates are thermal paths. They have surface properties, but not thermal mass properties. They account for incoming and outgoing radiation.

Radiating Plate The radiating plate module is a thermal path. This means that it is connected to at least one thermal node and its role is to calculate a heat rate into and out of that node via radiation. It accounts for solar heating, solar radiation reflected by Earth albedo, planetary infrared radiation, eclipses, and outgoing radiation. It is a quasi-1D model which has a location within a spacecraft, a surface normal vector, and an area. It can process additional user-specified fluxes in order to handle un-modeled flux sources. The radiating plate module is illustrated in Figure 6.

The net heat rate, $\dot{q}$, out of the plate is taken to be:

$$\dot{q} = \dot{q}_{\text{temp}} - \dot{q}_{\text{add,IR}} - \dot{q}_{\text{add,vis}} - \dot{q}_{\text{flux,IR}} - \dot{q}_{\text{albedo}} - \dot{q}_{\text{sun}} \tag{5}$$

where

$$\dot{q}_{\text{temp}} = \sigma T_u^4 A \epsilon_{\text{IR}} \tag{6}$$

is the thermal IR radiation and σ is the Stephan-Boltzmann constant, $5.67 \times 10^{-8} \frac{W}{m^2 K^4}$. The variable T_u is the upstream node temperature, while A is the surface area of the radiating plate, and ϵ_{IR} is the infrared absorptivity of the surface material.

$$\dot{q}_{\text{add,IR}} = -F_{\text{add,IR}} \epsilon_{IR} A \tag{7}$$

Equation (7) is the additional heat in due to a flux specified by the user in the infrared, $F_{\text{add,IR}}$. This is used to capture any unmodeled flux or background radiation.

$$\dot{q}_{\text{add,vis}} = -F_{\text{in,vis}} \epsilon_{\text{vis}} \tag{8}$$

Equation (8) is the additional heat in due to a flux specified by the user in the visible spectrum and ϵ_{vis} is the absoprtivity in the visible spectrum. Now, for each radiation source shining on the plate, a view angle factor, α, is calculated as

$$\alpha = \begin{cases} \hat{\boldsymbol{n}}_{\text{source}} \cdot \hat{\boldsymbol{n}}_{\text{plate}} \leq 0 & 0 \\ \hat{\boldsymbol{n}}_{\text{source}} \cdot \hat{\boldsymbol{n}}_{\text{plate}} > 0 & \hat{\boldsymbol{n}}_{\text{source}} \cdot \hat{\boldsymbol{n}}_{\text{plate}} \end{cases} \tag{9}$$

where $\hat{\boldsymbol{n}}_{\text{source}}$ is the unit vector which points to the light source and $\hat{\boldsymbol{n}}_{\text{plate}}$ is the surface normal of the plate. When combined with the surface area of the plate, this provides an effective area that the radiation acts on to heat the plate. It is used below:

$$\dot{q}_{\text{flux,IR}} = -\epsilon_{\text{IR}} A \sum_i F_{i,\text{flux,IR}} \alpha_i \tag{10}$$

In Equation (10), i iterates over a list of infrared fluxes, $F_{i,\text{flux,IR}}$, and the associated view angle factors.

$$\dot{q}_{\text{albedo}} = -\epsilon_{\text{vis}} A \sum_j F_{j,\text{albedo}} \alpha_j \tag{11}$$

Equation (11) is similar to Equation (10) but with flux sources due to albedo, $F_{j,\text{albedo}}$, which are considered to be in the visible spectrum. When calculating the heat rate from the sun, F_{sun} is the visible spectrum flux from the sun:

$$\dot{q}_{\text{sun}} = -F_{\text{sun}} \epsilon_{\text{vis}} A \alpha_i \tag{12}$$

Environment

Earth Albedo The albedo model used roughly follows from NASA Technical Memorandum 104596 but uses only one area element which is half the surface of the earth.[13] This model treats albedo reflectance as entirely diffuse reflection. The intensity of flux that reaches the spacecraft, $F_{\text{Earth,alb}}$, is

$$F_{\text{Earth,alb}} = F_{\text{Sun,Earth}} \beta \frac{S A_{\text{Earth}}}{2\pi ||\boldsymbol{r}_{\text{sc,Earth}}||^2} \hat{\boldsymbol{r}}_{\text{Sun,Earth}} \cdot \hat{\boldsymbol{r}}_{\text{Sc,Earth}} \tag{13}$$

where $||\boldsymbol{r}_{\mathrm{sc,Earth}}||$ is the distance from the spacecraft to the center of Earth and β is the albedo factor. SA_{Earth} is the surface area of Earth. $F_{\mathrm{Sun,Earth}}$ is the solar flux at the Earth. $\hat{\boldsymbol{r}}_{\mathrm{Sun,Earth}}$ is the unit vector pointing from the Earth to the Sun. The unit vector $\hat{\boldsymbol{r}}_{\mathrm{Sc,Earth}}$ points from the Earth to the spacecraft. Additionally, the above equation is set to 0 if $\hat{\boldsymbol{r}}_{\mathrm{Sun,Earth}} \cdot \hat{\boldsymbol{r}}_{\mathrm{Sc,Earth}} \leq 0$ because the spacecraft is then not above a sunlit portion of Earth. The orbit radius in the denominator is a deviation from the technical memorandum which intends for the user to integrate over multiple differential areas, so the orbit altitude is used in a slightly different way. Some errors with this single-element implementation in tandem with Equation (11) are evident. For instance, any panel with a surface vector orthogonal to the spacecraft-earth heading vector is modeled without flux due to Earth albedo. In reality this surface may see light from a portion of Earth not directly under the spacecraft. The validity of this simplification grows with orbit altitude.

Earth Infrared The Earth is modeled as an isotropic black body radiator. The radiation intensity at the spacecraft from the Earth, $F_{\mathrm{earth,IR}}$, is

$$F_{\mathrm{earth,IR}} = \sigma T_{\mathrm{earth}}^4 \frac{r_{\mathrm{earth}}^2}{r_{\mathrm{sc,earth}}^2} \tag{14}$$

where r_{earth} is the mean equitorial radius of Earth and $r_{\mathrm{sc,earth}}$ is the distance from the spacecraft to the center of Earth. σ is again the Stephan-Boltzmann constant. For Earth, a temperature of 255 K gives about the right average total flux in orbit.

Solar Radiation The same module used to simulate Earth infrared radiation is used to simulate solar radiation heating. A temperature around 5780 K gives the correct total flux at Earth. A separate absorptivity, ϵ_{vis} is used for visible spectrum heating as shown in Equations (10) and (12).

Thermal System

The thermal system module handles interactions between other thermal modules. Figure 2 demonstrates a simple system with two nodes, a conductor, a radiating plate, and a boundary node. In this case, the thermal system passes the two internal node temperatures to the conductor (as an example). It also passes the conductor heat rate to the two nodes so that the temperature can be integrated. Much more complex networks can be formed with more nodes and more thermal paths per node.

THERMAL SYSTEM TESTING

All modules in the thermal system (internal, external, and environment) are unit tested. Output from the modules is compared to expected output calculated independently. The thermal system module is unit tested and shown to properly link modules while conserving energy. All modules are combined in a basic Basilisk thermal scenario. The results of the scenario are compared to expected values. All tests pass without error.

THERMAL UTILITIES

Several utility functions are available which build upon the basic Basilisk thermal modules to create more complex thermal networks in a convenient way. Square meshes are used to approximate cubic spacecraft so that geometry issues remain secondary to the primary goals.

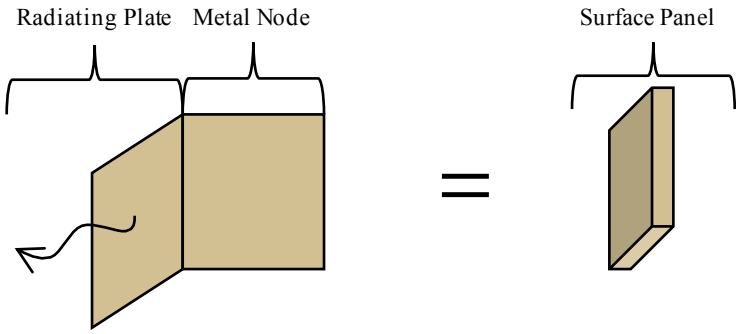

Figure 7. The surface panel utility conveniently sets up a surface element with both mass and radiative heat flow.

Surface Panel

The surface panel utility creates a square surface panel. A surface panel is an object which consists of a metal node connected to a radiating plate. In addition to creating an object to represent a spacecraft surface element, a surface panel adds features necessary for plotting a surface element. First, the shape of the surface element is created as a set of vertices within the panel's own reference frame. Second, the attitude of the panel frame relative to the spacecraft body frame is specified in 3-2-3 Euler angle coordinates. This happens to also define the panel surface normal, ${}^{\mathcal{B}}\hat{n}$, for radiation incidence factor calculations.

Meshed Square

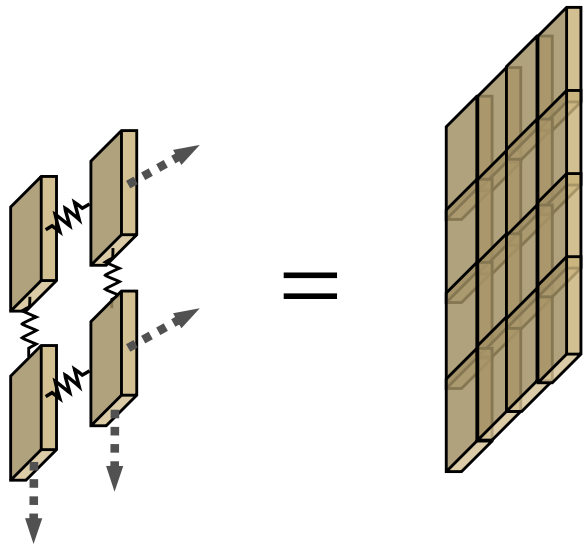

Figure 8. The meshed square utility links surface panels to create a meshed surface.

The meshed square utility creates a square panel which consists of smaller surface panels. The smaller panels inherit properties like attitude and mass from the larger panel so that they all have uniform properties. To modify the properties of individual elements, they can be referenced from

the meshed square's panel list and modified.

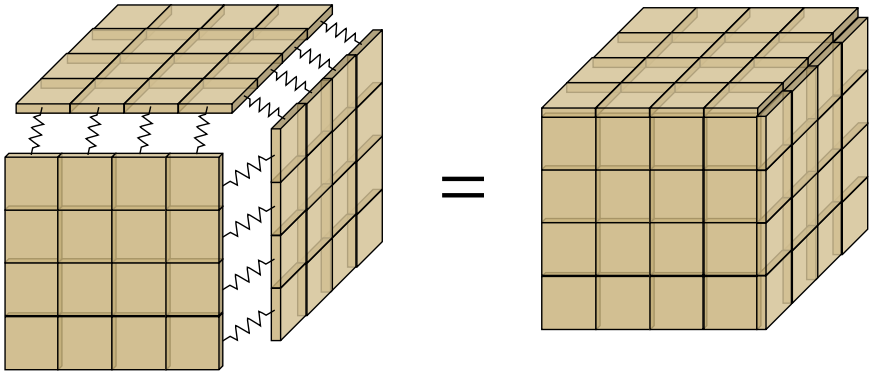

Figure 9. The meshed cube utility links six meshed squares to form a thermal meshed cube. This can be used to simulate the thermal surface of a cubesat. The user can control the mesh size.

Meshed Cube The meshed cube creates a thermal system of six interconnected meshed squares. Again, properties are derived from the cube inputs so that each side and all sub panels are uniform. Individual panel properties can be set by accessing them from each side's panel list. This is important because some panels may need to be connected to internal thermal system modules or modified such that they appear different to a thermal sensor. The meshed cube is useful because it provides a thermal model of a spacecraft of which the attitude is ambiguous in the visible spectrum, but may have defining features in the infrared.

INFRARED CAMERA MODULE

A prototype infrared camera module is written for Basilisk in Python, although the rest of the thermal system modules are written in C++. Aside from generally rapid development, Python provides the matplotlib plotting library which is used to make simulated thermal images.

Geometry Projection

The sensor uses a pinhole camera model perspective projection to generate images as seen in Figure 10. This means that, given a 3D point in the camera frame, $\boldsymbol{X}$, the points projected onto the image plane $\boldsymbol{X}'$ are :

$$\begin{bmatrix} X_1' \\ X_2' \end{bmatrix} = -\frac{f}{X_3} \begin{bmatrix} X_1 \\ X_2 \end{bmatrix} \tag{15}$$

If the third element of $\boldsymbol{X}$ is included in the calculation then the third element of $\boldsymbol{X}'$ is always $-f$ which shows that this projection is really calculating the intersection of camera-pinhole-to-object lines with the image plane in the camera coordinate system. The projection equation can be derived by looking at similar triangles in Figure 10.

Camera Placement

The thermal camera is intended to be placed onto one spacecraft and aimed at another. Its placement within the observer spacecraft is specified by position and attitude. By default the camera pupil frame is coincident with the spacecraft body frame. Other positions are specified by the ${}^{\mathcal{B}}\boldsymbol{r}_{PB}$ attribute which is the position of the Pupil frame within the Spacecraft body frame. The attitude of

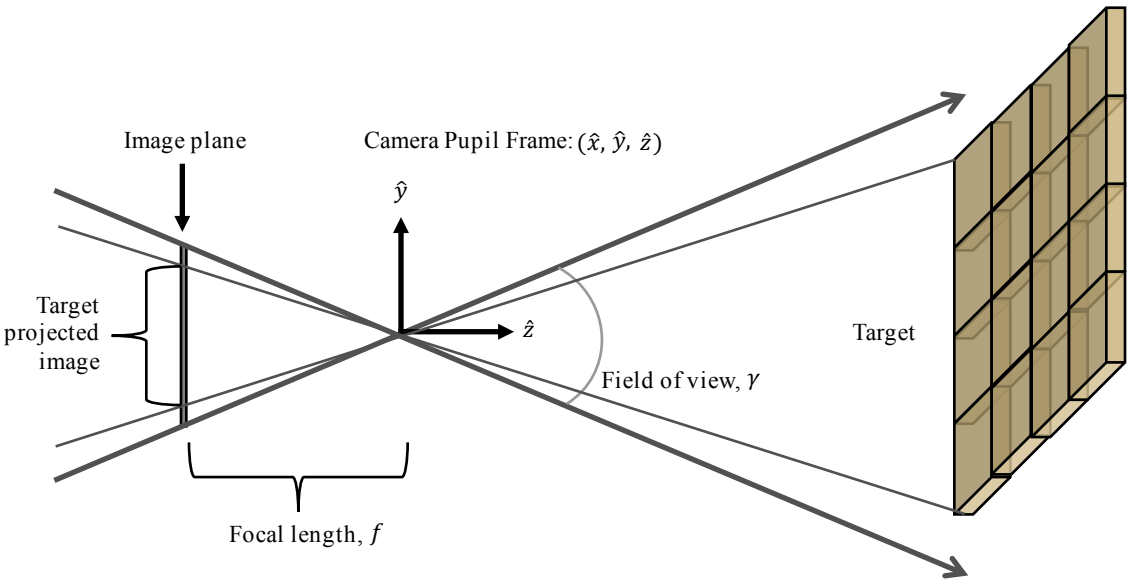

Figure 10. The pupil frame is oriented so that the more distant objects are in the $+\hat{z}$ direction.

the camera is specified by the $\boldsymbol{\sigma}_{PB}$ which specifies the Modified Rodriguez Parameter between the same two frames.

Intrinsic Parameters

Focal Length Focal length, f, specifies the distance from the camera pupil to the image plane. The true image plane lies at $-f\hat{\boldsymbol{z}}$.

Field of View The field of view angle, γ of the camera is specified. Together with the focal length, the field of view determines the size of the detector array, l, which is assumed square.

$$l = f \tan\left(\frac{\gamma}{2}\right) \tag{16}$$

Pixels The number of pixels can be set by the user. Only a symmetric number of pixels is accounted for.

Geometry Inputs and Calculations

The camera is given panel 3-D vertices, panel attitudes with respect to the body, panel temperatures, panel surface vectors ${}^{\mathcal{B}}\hat{\boldsymbol{n}}$, and spacecraft position and attitude. The geometry 3-D vectors (surface vectors and vertices) are stored as $3 \times 4M$ matrix of horizontally stacked vectors. In this way, the module takes advantage of python vectorization and avoids `for` loops. For instance

$${}^{P}\boldsymbol{r}_{CP} = [PN][NB]{}^{B}\boldsymbol{r}_{CP,3\times 4M} \tag{17}$$

projects the 3-D corner vectors of the M target surface panels, ${}^{B}\boldsymbol{r}_{CP,3\times 4M}$, with respect to the camera pupil from the body frame into the pupil frame in one fell swoop. Similarly, all of the points

can be projected from 3-D to the 2-D image plane per Equation (15) in a single call because the $\boldsymbol{X}$ and $\boldsymbol{X}'$ vectors are horizontally stacked.

Temperature Visualization

Temperatures are read from the thermal system for each panel at every time step. A maxmimum and minimum temperature are specified for the camera. The maximum, minimum, and current panel temperatures are used as inputs to a colormap to determine which color the panel should be.

Plotting the Image

For each panel in the system, a square is added to a plot during initialization with four points and a default color as a PolyCollection*. These PolyCollections are stored in a list. Then, during each image update, all of the PolyCollection vertices are set to the computed image plane projected geometry points. The z-order of the polygons is set as the negative of the maximum z-coordinate of the 3-D panel points in the pupil frame. Finally, the color of each panel is set using the thermal colormap. When the image is generated, the x-axis is reversed. This is done so that the depth of the image (into the image) completes a right handed camera pupil frame.

Using the Image

The camera module has the option to save each image with a simulation time-stamp to a specified filepath as a `.png`. Otherwise, the images are written as byte-string rgb bitmaps to the Basilisk Messaging System where they are held in memory. They can then be used real time by visual navigation modules or read out of memory at the end of the simulation. The messaging option is faster, but uses more memory. For more information on the Basilisk messaging system, please see the most recent documentation.[14]

INFRARED CAMERA EXAMPLE SCENARIO

Table 1. Camera Parameters Used

parameter	value
field of view	30 (deg)
focal length	10 (cm)
max temp	350 (K)
min temp	250 (K)
3-2-3 Euler Angles	(0, 0, 0) (deg)
position in observer	$[0, 0, 0]^T$ (m)

A scenario is set up in Basilisk to demonstrate the working infrared camera module as shown in Figure 1. Figure 11 shows the set-up of the Basilisk modules in the simulation. The scenario involves two spacecraft: the target and the observer. The target spacecraft has a thermal system with a meshed cube attached to it. A hot spot is created by adding an additional constant heat flow to one panel on the target spacecraft. The observer spacecraft has a camera attached to it. The camera parameters used are shown in Table 1. The scenario is set up such that the observer and target are closing on each other while the target moves to the side and is spinning. The series

*The original intent was to use mplot3d and Poly3DCollection. These packages perform the projection under the hood. However, the input most closely resembling focal length (`.dist`) does not work exactly like a focal length. The 3-D library sometimes produces images that require trimming before analysis.

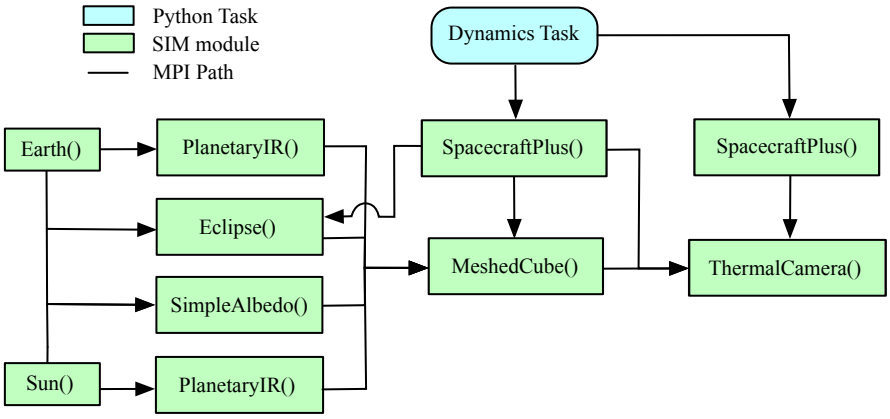

Figure 11. This block diagram of the camera scenario shows the relationship of the Basilisk modules used to model a thermal imaging scenario. The arrows show the routing of data via the Message Passing Interface (MPI).[14]

of images in Figure 12 demonstrates this scenario. A larger mesh would cause the heat to spread smoothly. This scenario demonstrates the basic capabilities of the Basilisk thermal system to model a combination of internal and external thermal coupled with multi-spacecraft dynamics and thermal sensors.

CONCLUSION

A prototype infrared camera module has been built and demonstrated in the Basilisk astrodynamics framework. Building and testing this module required building and testing a lumped-parameter thermal network before work on the camera could be started. All necessary elements of the modular thermal network solver and camera are in place and working for simple scenarios. Some thermal vision navigation work could be done with these packages. However, further work should be done to develop higher fidelity thermal network and sensor modules.

The primary thrust of work on the thermal network solver should be in coupling the thermal dynamics with the spacecraft dynamics. Currently, the thermal system does its own Euler integration, but it should be added to the Basilisk state engine. This will allow closely coupled thermal dynamics and dynamics. Additionally, algorithm improvements can be made to the way the system manages thermal states. Next, work should be done to interface the Basilisk thermodynamics system with a standard CAD output format so that real, complex spacecraft geometry can be input. Finally, improvements should be made to the environmental models. Particularly, the albedo module should be expanded to using a meshed planet surface to integrate albedo flux.

The camera should plot the flux received from each surface. There is a scrambling of information when heat is radiated as temperature to the fourth power and degraded by the inverse square law as it travels to the camera. This is not accounted for now. Furthermore, there are corruptions internal and external to the camera that need to be modeled.

ACKNOWLEDGEMENT

This work is supported by a Draper Graduate Research Fellowship.

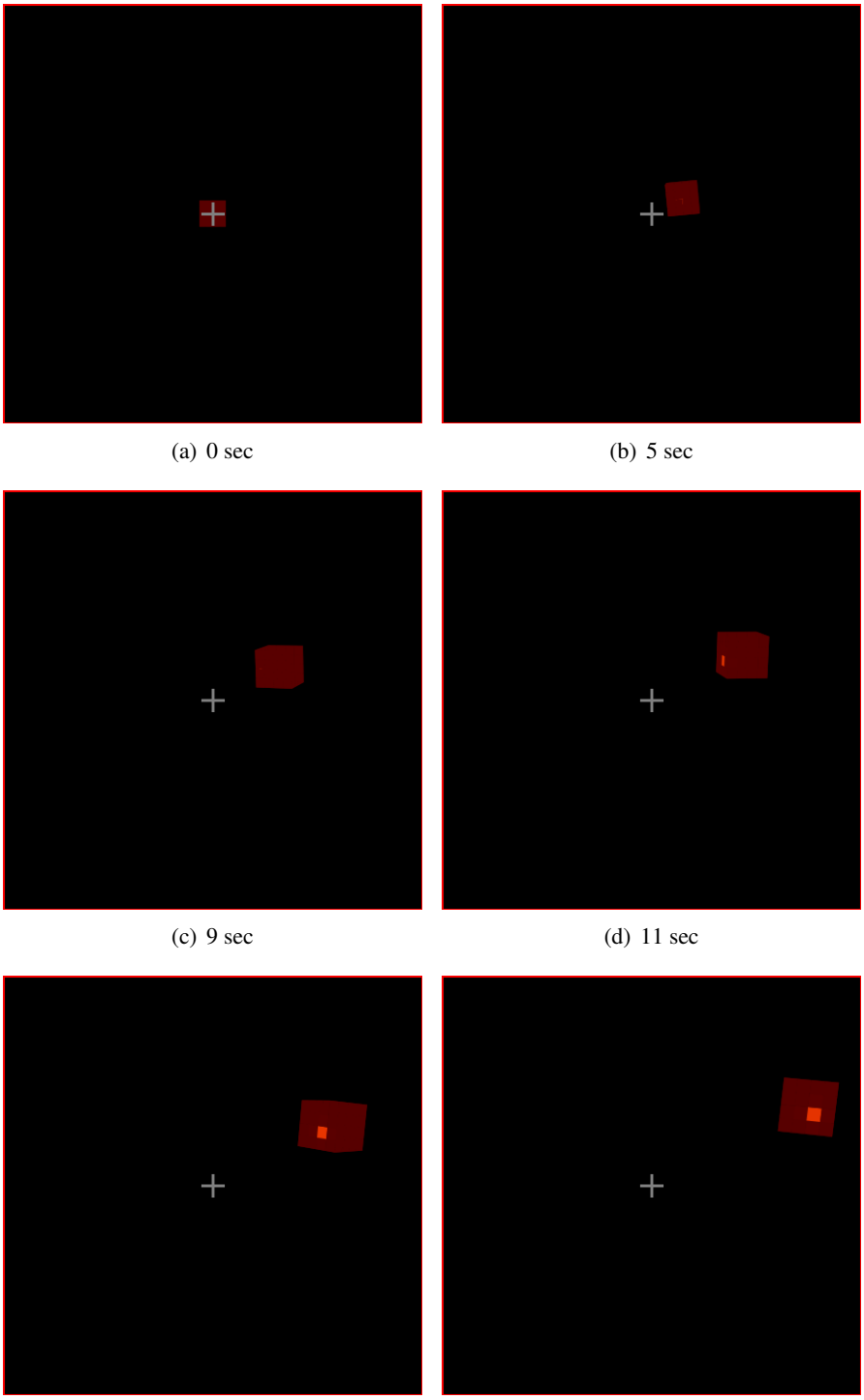

(a) 0 sec (b) 5 sec

(c) 9 sec (d) 11 sec

(e) 13 sec (f) 15 sec

Figure 12. A series of infrared images in a two-spacecraft simulation. The target spacecraft has a hotspot that is initially facing away from the observer, but this comes into view as the target spins and flies past the observer.

REFERENCES

[1] O. Yilmaz, N. Aouf, L. Majewski, M. Sanchez-Gestido, and G. Ortega, "Using infrared based relative navigation for active debris removal," *10th International ESA Conference on Guidance, Navigation & Control Systems*, 2017.

[2] C. R. McBryde and L. E. Glenn, "Spacecraft Relative Navigation Using Appearance Matching and Sensor Fusion," *Proceedings of the 2017 International Technical Meeting of The Institute of Navigation*, 2017.

[3] C. R. McBryde and E. G. Lightsey, "End-to-End Testing of a Dual Use Imaging Sensor for Small Satellites," *Journal of Small Satellites*, Vol. 5, 2016, pp. 435–448.

[4] J. Richmond, "Adaptive Thermal Modeling Architecture For Small Satellite Applications," Master's thesis, Massachusetts Institute of Technology, Cambridge, MA, 2010.

[5] C. Garnier, R. Collorec, J. Flifla, C. Mouclier, and F. Rousee, "Infrared sensor modeling for realistic thermal image synthesis," *1999 IEEE International Conference on Acoustics, Speech, and Signal Processing. Proceedings. ICASSP99 (Cat. No.99CH36258)*, Vol. 6, 04 1999, pp. 3513–3516 vol.6, 10.1109/ICASSP.1999.757600.

[6] J.-F. Shi, S. Ulrich, S. Ruel, and M. Anctil, "Uncooperative Spacecraft Pose Estimation Using an Infrared Camera During Proximity Operations," *AIAA Space 2015 Conference and Proceedings*, https://doi.org/10.2514/6.2015-4429, AIAA SPACE Forum, 2015.

[7] J. Ventura, A. Fleischner, and U. Walter, "Pose Tracking of a Noncooperative Spacecraft During Docking Maneuvers Using a Time-of-Flight Sensor," *AIAA Guidance, Navigation, and Control Conference*, https://doi.org/10.2514/6.2016-0875, AIAA SciTech Forum, 2016.

[8] B. Cavrois, A. Vergnol, A. Donnard, P. Casiez, and O. Mongrard, "LIRIS demonstrator on ATV5: a step beyond for European non cooperative navigation system," *AIAA Guidance, Navigation, and Control Conference*, https://doi.org/10.2514/6.2015-0336, AIAA SciTech Forum, 2015.

[9] J.-F. Shi, S. Ulrich, and S. Ruel, "Spacecraft Pose Estimation using Principal Component Analysis and a Monocular Camera," *AIAA Guidance, Navigation, and Control Conference*, Grapevine, Texas, AIAA SciTech Forum, 2017.

[10] T. Teil and H. Schaub, "Software Architecture For Closed-Loop Autonomous Optical Navigation Scenarios," *1st Annual RPI Workshop on Image-Based Modeling and Navigation for Space Applications*, Troy, NY, June 4–5 2018.

[11] TRW Systems, "Thermal Network Modeling Handbook," Tech. Rep. 9-10435, TRW Systems, 1972.

[12] K&K Associates, "Thermal Network Modeling Handbook Reformatted," Tech. Rep. , K&K Associates, 2000.

[13] T. W. Flatley and W. A. Moore, "An Earth Albedo Model: A Mathematical Model for the Radiant Energy Input to an Orbiting Spacecraft Due to the Diffuse Reflectance of Solar Radiation from the Earth Below," *NASA Technical Memorandum*, No. 104596, 1994, pp. 1–3.

[14] P. W. Kenneally, S. Piggott, and H. Schaub, "Basilisk: A Flexible, Scalable and Modular Astrodynamics Simulation Framework," *7th International Conference on Astrodynamics Tools and Techniques (ICATT)*, DLR Oberpfaffenhofen, Germany, Nov. 6–9 2018.